Article │ Received 22 May 2025; Accepted 15 July 2025; Published 11 August 2025
https://doi.org/10.55092/ae20250008

Microstructure evolution and property improvement of Al–Zn–Mg–Cu alloy processed by laser-arc hybrid additive manufacturing

Dehua Liu[1,*], Jiang Bi[2], Zhuoyun Yang[2] and Guojiang Dong[2]

[1] State Key Laboratory of Crane Technology, Yanshan University, Qinhuangdao 066004, China
[2] Key Laboratory of Advanced Forging & Stamping Technology and Science of Ministry of Education, Yanshan University, Qinhuangdao 066004, China

* Correspondence author; E-mail: ldh@ysu.edu.cn.

Highlights:

- We proposed a feasible approach of combination for laser-arc hybrid process and subsequent heat treatment to manufacture the Al–Zn–Mg–Cu alloy with superior mechanical properties.
- The strength-ductility balance with ultimate tensile strength of 590 MPa and elongation of 8.6% was achieved.
- Compared to the LAHAM-processed specimen, the ultimate tensile strength and yield strength in the heat-treated specimen were enhanced by approximately 87% and 169%.

Abstract: Recently, laser-arc hybrid additive manufacturing (LAHAM) has emerged as a promising strategy for fabricating components with favorable performance. In this paper, we compared the microstructure and mechanical properties of Al–Zn–Mg–Cu alloy manufactured by wire + arc additive manufacturing (WAAM) and LAHAM and obtained strengthening by means of heat treatment. The microstructure consisted of coarse columnar grains with an average grain size of 70.4 μm in the WAAM-processed Al–Zn–Mg–Cu alloy. Compared to the WAAM specimen, the grain size of LAHAM specimen was reduced by 68%, and the eutectics distribution was more uniform. The high-densities η' precipitates with the length of 10–30 nm appeared in the processed by LAHAM. The key achievement indicated that the ultimate tensile strength (590 ± 9 MPa) and elongation (8.6 ± 0.2%) for LAHAM-processed Al–Zn–Mg–Cu alloy after heat treatment were enhanced by approximately 87% and 169% than those in the deposited specimen.

Keywords: high-strength aluminum alloy; microstructure evolution; laser-arc hybrid additive manufacturing; heat treatment

1. Introduction

In the contemporary epoch of rapid industrial revolution, there is an increasingly demand for innovative engineering materials. Consequently, it becomes essential to transition modern manufacturing into a new period defined by low costs and increased convenience [1]. Additive manufacturing (AM) eliminates the need for traditional cutting tools, fixtures, and multiple processing steps, enabling rapid fabrication of complex-shaped components with tailored microstructures and macro-properties. When compared to traditional subtractive and other equivalent manufacturing processes, AM can realize the customized design of structure, internal microstructure, and macro property of products. Especially, it enjoys unique advantages in shortening the processing cycle and reducing manufacturing costs.

Al–Zn–Mg–Cu alloy represents a kind of high-strength aluminum alloy, which is primarily employed in metal components that require exceptional strength, toughness, and damage resistance [2]. Obviously, AM can directly produce large-scale complex Al–Zn–Mg–Cu alloy components, which are difficult to achieve through traditional manufacturing methods. As such, this innovation has attracted increasing attention in many industrial fields and expected to bring new advancements in the preparation of aluminum alloys [3]. However, unlike the titanium or nickel-based alloys that are suitable for AM, the range of solid-liquid phase transition temperatures in the Al–Zn–Mg–Cu alloy is extensive because of its chemical composition. Furthermore, the notable temperature gradient, cooling speed, and other solidification conditions linked with AM might encourage the formation of large columnar grains and heighten the risk of cracking [4]. Qi *et al.* investigated the crack defect in the 7050 aluminum alloy utilizing laser power bed fusion (LPBF) and discovered that high-density deposited specimen could be obtained via optimized process. Unfortunately, the crack defect remains unavoidable [5]. In summary, LPBF is not considered suitable for Al–Zn–Mg–Cu alloy because its mechanical properties are usually lacking. So far, many researches have focused on improving the microstructure and performance of Al–Zn–Mg–Cu alloy fabricated via WAAM by changing process parameters, including arc mode, deposition rate, and wire feed speed, *etc.* [6]. Dong *et al.* studied WAAM-processed Al–Zn–Mg–Cu alloy, finding that the deposited specimen had coarse grains. Additionally, the ultimate tensile strength and elongation were poor with only 230.7 MPa and 3.3%, respectively [7]. Moreover, achieving a high-performance Al–Zn–Mg–Cu alloy component via AM is tough without follow-up heat treatment or other reinforcement strategies.

Recent investigations have predominantly concentrated on novel methods for enhancing the property of high-strength aluminum alloy through hybrid additive manufacturing techniques [8]. Notably, LAHAM have demonstrated substantial benefits in improving forming efficiency, minimizing defects, and refining grains. Wu *et al.* established that the enhanced strength of the Al–Cu alloy, fabricated via laser-arc hybrid methods, was due to the uniform arrangement of eutectics and precipitates in the laser zone [9]. Liu *et al.* displayed the advantages of LAHAM and further elucidated the grain refinement mechanism, highlighting its beneficial effect on property enhancement [10]. Gong *et al.* employed LAHAM to prepare stainless steel and controlled the microstructure by varying the laser power [11]. However, previous studies on LAHAM were limited to aluminum alloy with lower strength. For the fabricating high-strength Al–Zn–Mg–Cu alloy, some challenges remain urgent to be solved, such as microstructure control and mechanical properties improvement.

In this study, we analyzed the macroscopic forms of Al–Zn–Mg–Cu alloy created through WAAM and LAHAM, while also discussing the evolution of grain morphology and secondary phases. The heat

treatment that followed further improved the mechanical properties of the deposited Al–Zn–Mg–Cu alloy. This study aims to broaden the current research on Al–Zn–Mg–Cu alloy and provide new strategies for microstructure design and property improvement.

2. Material and methods

In our research, a designed Al–Zn–Mg–Cu alloy welding wire was utilized as the deposited material. The detailed chemical composition of filler wire and as-deposited specimen are listed in Table 1. The substrate was selected as 7075 aluminum alloy plate with dimensions of 200 mm × 200 mm × 15 mm. As illustrated in Figure 1a, the AM proceeding was facilitated via the LAHAM system, comprising of a Nd:YAG pulsed laser, a Miller arc welding machine, an automatic wire feeder, and a CNC machine. We have fabricated the thin-walled Al–Zn–Mg–Cu alloy was fabricated by reciprocating scanning strategy (returning to the starting position after single-layer scanning). Other parameters related to the LAHAM process are detailed in Table 2. To investigate the effect of subsequent heat treatment on the microstructure and mechanical properties of Al–Zn–Mg–Cu alloy, the deposited specimens were initially heated to 450 ℃ and maintained for 2 h. Subsequently, they were further heated to 475 ℃ and kept for 2 h, and finally quenched in cold water to complete the solution treatment. The aging treatment was conducted at 120 ℃ for 48 hours.

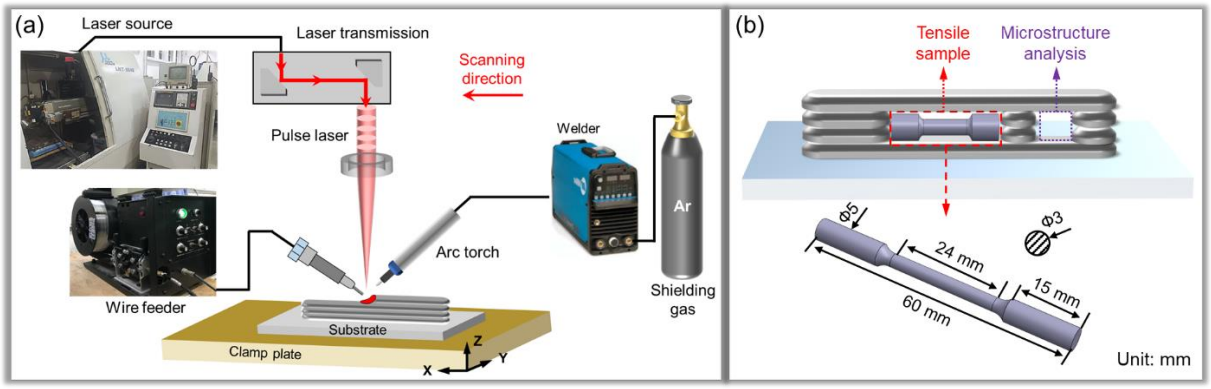

Figure 1. Schematic drawings of experimental process and deposited specimen: **(a)** the laser-arc hybrid additive manufacturing system, **(b)** sampling positions of microstructure and tensile specimens.

Table 1. Main chemical compositions of filler wire and as-deposited specimen (wt %).

Element	Al	Zn	Mg	Cu	Fe	Cr	Zr	Mn
Filler wire	Bal.	7.75	1.46	2.34	0.08	0.02	0.12	0.01
As-deposited specimen	Bal.	7.47	1.82	2.37	0.07	0.02	0.11	0.01

Table 2. Typical process parameters in this work.

	WAAM	LAHAM
Laser power (W)	--	150
Pulse frequency (Hz)	--	30
Single pulse energy (J)	--	5
Arc current (A)	120	120
Scanning speed (mm/min)	250	250
Wire feed speed (mm/min)	1500	1500
Ar protective gas flow (L/min)	15	15

The metallographic and tensile samples were extracted from the thin-walled specimen using electrochemical machining. The metallographic sample was polished and subsequently etched with Keller reagent. The macro morphology and surface roughness of deposited specimen were characterized by laser confocal microscope (Zeiss, LSM900). The Hitachi scanning electron microscope (SEM, SU5000) equipped with an energy dispersive X-ray spectrometer (EDS) was utilized to observe the microstructure and fracture morphology. The grain orientation was collected via electron backscatter diffraction (EBSD) and the corresponding data were analyzed by AztecCrystal software. For the investigation of nano-scaled precipitates, the transmission electron microscopy (TEM) sample thinning was prepared with focused ion beam (FIB, Helios 5 Hydra UX) and detected using a field emission scanning transmission electron microscope (JEOL, JSM-F200). The uniaxial tensile test was conducted on an electronic universal testing machine (Instron 5982) equipped with extensometers. As shown in Figure 1b, the test samples were machined into the dog bone shape, and the tensile speed was set to 1 mm/min.

3. Results and discussions

3.1. Macrostructure

The LAHAM process integrates the energy characteristics of both laser and arc, demonstrating significant distinctions. Hence, the energy distribution within the molten pool affects the shape and microstructure of the deposited Al–Zn–Mg–Cu alloy, and this part will explore its impact on the macrostructure of WAAM and LAHAM processes. Single-layer and multi-layer Al–Zn–Mg–Cu alloy specimens are analyzed for forming quality based on their cross-section and side surface characteristics. As shown in Figure 2, the deposited specimens exhibit no crack defects. For the WAAM-processed specimen, the cross-sectional fusion zone of single-layer display a central fusion configuration, with molten height and depth being shallower (Figure 2a). Furthermore, the surface roughness of deposited thin-walled specimen is measured at S_a = 27.2 μm. Whereas, the laser-arc hybrid layer has large height-to-width ratio due to molten pool diffusion driven by the laser beam, as depicted in Figure 2b. The molten depth increases from 2.0 mm to 3.1 mm, while its width expanded from 5.0 mm to 5.2 mm. This demonstrates that laser-arc hybrid has significant capability for regulating the size of deposited specimen. There is an overflow at the thin-walled specimen can be observed via the LAHAM, leading to a slight increase in surface roughness to S_a = 31.1 μm. Notably, due to the diameter of laser beam is only 0.6 mm, the deposited layer in Figure 2c exhibits a shape characterized by a wide upper region and a narrow bottom region, which results in higher energy density in the central region compared to the side. Tani *et al.* [12] and Gao *et al.* [13] similarly identified comparable molten pool characteristics in the investigation of laser-arc hybrid welding. For clarity, this research defines the upper region of molten pool as the arc zone (AZ), and the bottom region as the laser zone (LZ).

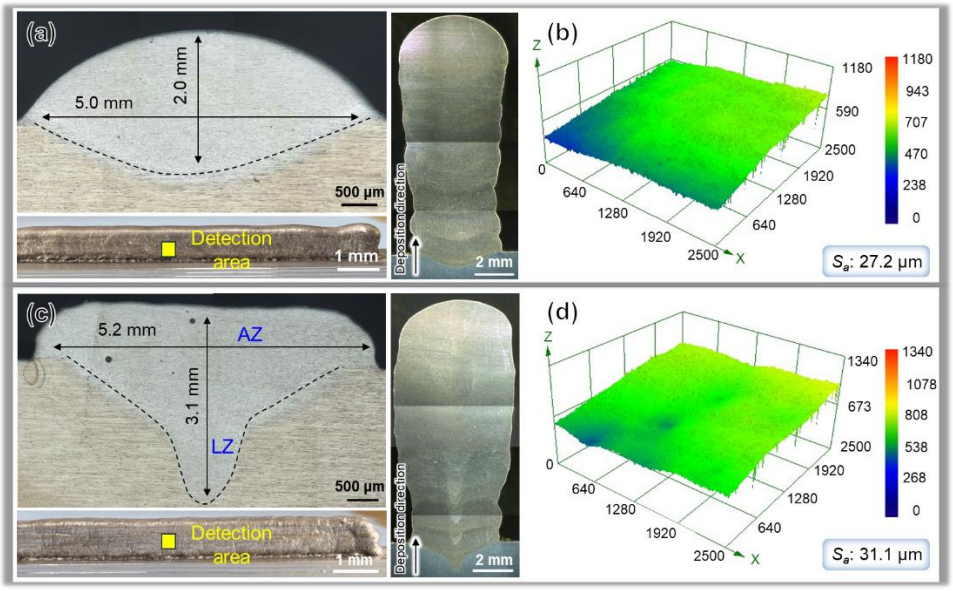

Figure 2. Macrostructure analysis: **(a)** cross-sectional of WAAM-processed Al–Zn–Mg–Cu specimen; **(b)** surface morphology of deposited thin wall; **(c)** cross-sectional of LAHAM-processed specimen; **(d)** surface morphology of deposited thin wall.

3.2. Microstructure analysis

Figure 3 depicts the EBSD images of deposited Al–Zn–Mg–Cu alloy fabricated by WAAM and LAHAM. To depict the grain morphology along the deposition direction in the middle of the WAAM and LAHAM specimens, EBSD analysis is performed. As indicated in Figure 3a, microstructure consists of coarse columnar grains with an average grain size of 70.4 μm, and the maximum grain diameter reaches 600 μm. This is the typical microstructure feature of WAAM-processed Al–Zn–Mg–Cu alloy, in accordance with the studies of Dong *et al.* [7]. From the solidification principle [14], the initiation of crystallization at the molten pool's bottom boundary, where the temperature gradient to solidification rate ratio is high, results in continuous columnar grain growth towards the center. During grain growth in Al–Zn–Mg–Cu alloy, the crystallographic orientation is primarily along the <100> direction and perpendicular to the isotherms at the molten pool boundary, where heat dissipates more quickly. Conversely, the growth along the boundary isotherm direction is inhibited, generating the columnar grain with epitaxial growth along the deposition direction. This can also be confirmed by the polar figure. As presented in Figure 3b, the Al–Zn–Mg–Cu alloy processed by LAHAM exhibits a significant change in grain morphology, producing a bimodal grain size distribution with alternating columnar grains in the AZ and equiaxed grains in the LZ. The proportion of equiaxed grain increases to 55%. It is noteworthy that the grain distribution in the LAHAM specimen exhibits a greater concentration than that of WAAM specimen, and the grain diameters are mainly distributed in the range of 5 μm to 50 μm. In comparison to the WAAM specimen, the average grain size is reduced by approximately 68%. The increased temperature gradient (G) and solidification rate (R) in the LZ, associated with a supercooling area, lead to a larger $G \times R$, which promotes the development of a fine grain zone at the base of the molten pool. Additionally, laser stirring disrupts dendrites, which then serve as nucleation sites, yielding a finer microstructure. Unlike the WAAM-processed Al–Zn–Mg–Cu alloy, the LAHAM specimen features equiaxed grains with random and uniform orientation, and the pole density decreases to 3.8, showing no texture orientation

(Figure 3b). Consequently, the LAHAM process appears to facilitate changes in the morphology of grains. According to Read and Shockley *et al.* [15], equiaxed grains have high-angle grain boundaries that are low in energy, effectively impeding dislocation movement during deformation and contributing to enhanced strength.

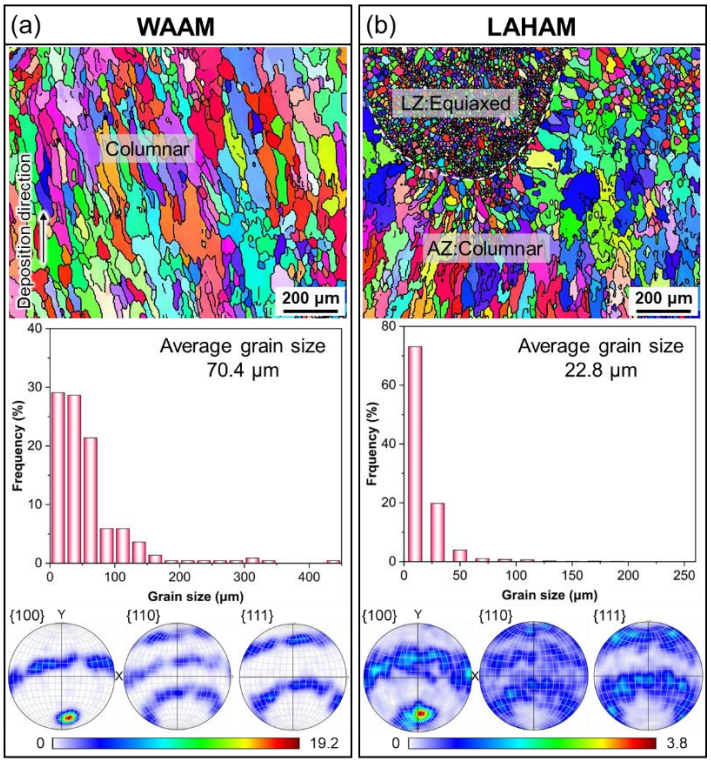

Figure 3. The EBSD image of microstructure with different additive manufacturing methods: **(a)** WAAM; **(b)** LAHAM.

The mechanical properties and fracture behavior of specimens made by WAAM and LAHAM are significantly influenced by the morphology and distribution of the secondary phase. Accordingly, SEM characterization of secondary phase was carried out. Figure 4a shows an SEM image of columnar grains in the Al–Zn–Mg–Cu alloy processed by WAAM. A continuously distributed secondary phase is visible at the columnar grain boundary, with a granular phase scattered inside the grain. The secondary phase, both at the grain boundary and within the grain, is examined using EDS, revealing a similar elemental makeup, predominantly containing Zn, Mg, and Cu. Combined with the lamellar feature, it is inferred to be eutectics consisting of α-Al+η-$MgZn_2$. Generally, it is broadly acknowledged that the precipitation sequence of the secondary phase in the Al–Zn–Mg–Cu alloy follows α-Al → GP zone → η'-$MgZn_2$ → η-$MgZn_2$ [16]. Yang *et al.* [17] revealed that Al and Cu atoms could easily replace the Zn atom and dissolve into the η phase. Thus, the η phase can also be expressed as η-$Mg(Zn,Cu,Al)_2$. Figure 4b shows the SEM image at junctions of AZ and LZ in the LAHAM-processed Al–Zn–Mg–Cu alloy. Notably, there are significant changes in the eutectics within the AZ and LZ, where the eutectics along the grain boundaries in the AZ become finer. The most exciting feature in the LZ is the uniformly distributed eutectics within the grain. This indicates that laser-arc hybrid can promote the homogenization of eutectics.

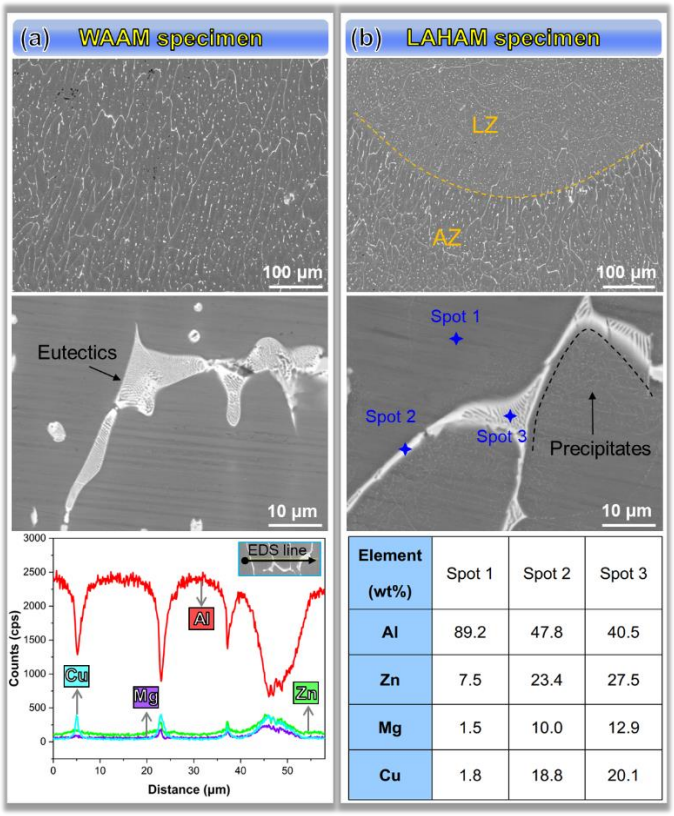

Element (wt%)	Spot 1	Spot 2	Spot 3
Al	89.2	47.8	40.5
Zn	7.5	23.4	27.5
Mg	1.5	10.0	12.9
Cu	1.8	18.8	20.1

Figure 4. The SEM and EDS results of secondary phase in the deposited specimen: **(a)** WAAM specimen; **(b)** LAHAM specimen.

Figure 5 reveals the microstructure of Al–Zn–Mg–Cu alloy prepared via LAHAM after solid solution and aging treatment. In comparison to deposited specimen, the continuous secondary phase located at the grain boundaries is disrupted, whereas the presence of rod-like or spherical secondary particles within the grains is enhanced (Figure 5a). Moreover, it becomes challenging to identity the AZ and LZ based on the characteristics of secondary phase. From the EDS mapping in Figure 5b, these particles are indicated as Al_2CuMg. It is noted that Zn diffuses through α-Al at a much higher coefficient compared to Mg and Cu at equivalent temperatures [18]. Owing to the rapid diffusion rate, Zn preferentially diffuses into α-Al, while Mg and Cu remain in the eutectics, which eventually transforms into the Al_2CuMg. As is well known, the high strength of Al–Zn–Mg–Cu alloy primarily comes from the precipitation strengthening of nano-scaled precipitates. Furthermore, the precipitates are analyzed by TEM, and some details are shown in Figure 5c. To examine the nano-scale phase, the TEM sample is collected from the middle section of the as-deposited and heat-treated specimens. After heat treatment, the Al–Zn–Mg–Cu alloy processed by LAHAM shows high-density precipitates with lengths of 10–30 nm, which are identified as the η' phase through selected area electron diffraction (SAED). Moreover, the high-resolution transmission electron microscope (HRTEM) reveals that the η' precipitates interact strongly with dislocations, serving as an impenetrable barrier to slip dislocations.

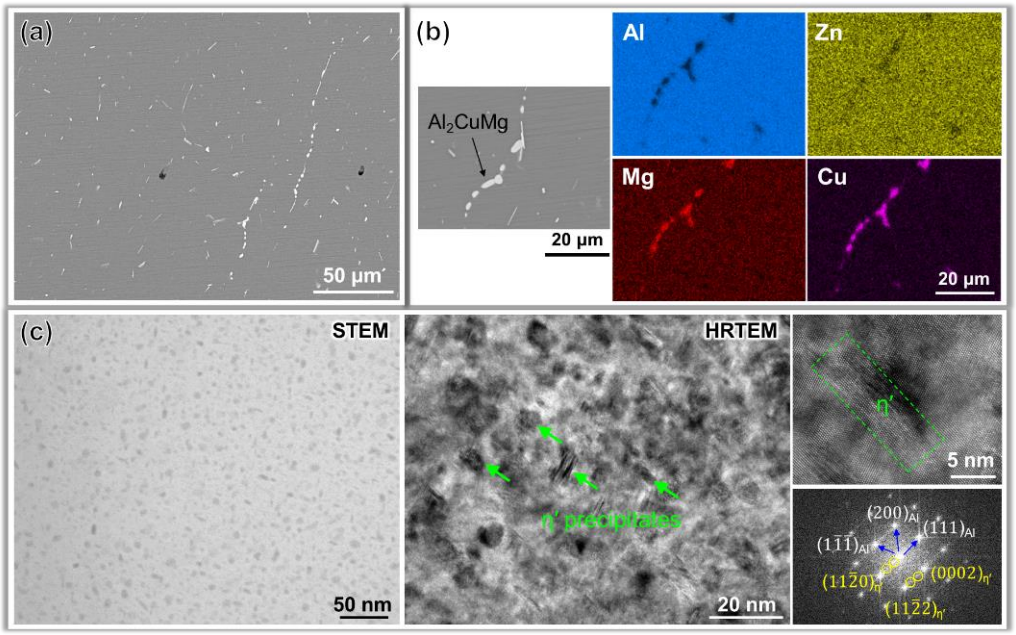

Figure 5. Secondary phase and nano-scaled precipitate analysis after heat treatment: **(a)** SEM image; **(b)** element distribution; **(c)** STEM and HRTEM images of η' precipitate.

3.3. Mechanical properties and fracture morphologies

The mechanical characteristics of specimens produced through WAAM and LAHAM, prior to and following heat treatment, are depicted in Figure 6a. The LAHAM-processed Al–Zn–Mg–Cu alloy have comparatively favorable tensile properties with ultimate tensile strength (UTS) of 315 ± 11 MPa and yield strength (YS) of 226 ± 11 MPa, which are 13% and 16% higher than those of WAAM specimen (UTS = 279 ± 12 MPa and YS = 195 ± 9 MPa). However, achieving both strength and ductility in Al–Zn–Mg–Cu alloy is not feasible, as increasing strength results in reduced ductility. Thus, the elongation is slightly reduced to 3.2 ± 0.1%. Following heat treatment, the mechanical properties of both WAAM and LAHAM specimens exhibited significant improvements as expected. For the WAAM specimen, the UTS increases from 279 MPa to 526 MPa and maintained 7.7% elongation. Noticeably, comparing with the deposited Al–Zn–Mg–Cu alloy, the UTS and elongation of LAHAM specimen treated with aging for 48 h increase of 87% and 169%, achieving values of 590 ± 9 MPa and 8.6 ± 0.2%, respectively. This demonstrates that the LAHAM-processed Al–Zn–Mg–Cu alloy not only have great formability, as well as exhibit excellent strength-ductility matching performance. In Figure 6b, the UTS and elongation from this research are compared to the Al–Zn–Mg–Cu alloy created by LPBF and WAAM in past reports. Evidently, the Al–Zn–Mg–Cu alloy processed by LAHAM exhibits greater strength compared to those produced by other methods, offering potential benefits in various applications.

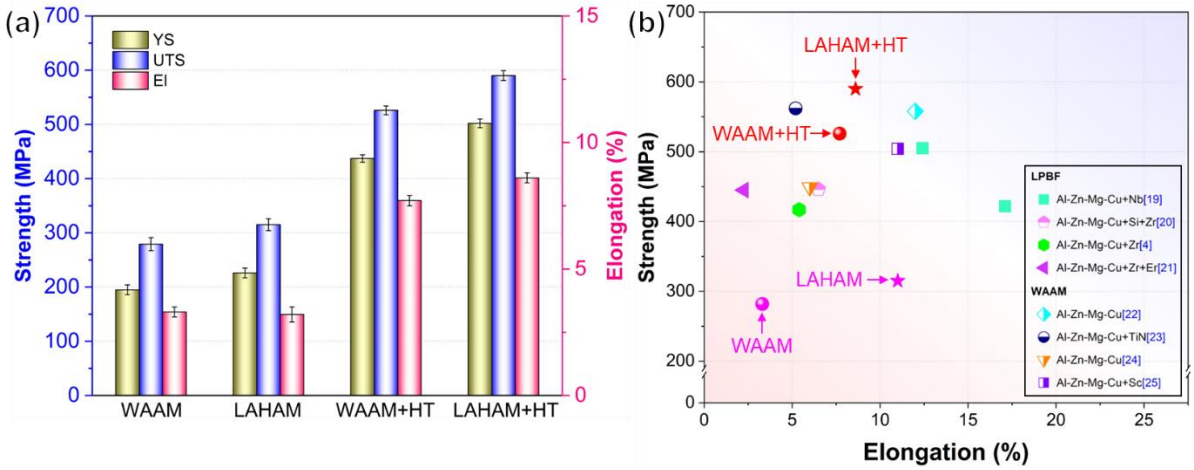

Figure 6. Tensile properties of Al–Zn–Mg–Cu alloy before and after heat treatment: **(a)** the statistics of tensile test results; **(b)** Comparison of the tensile strength and elongation from the literature [19–25] for AM-processed Al–Zn–Mg–Cu alloy.

The usual fracture appearances of the Al–Zn–Mg–Cu alloy in deposited and heat-treated specimens are displayed in Figure 7. The fracture in the WAAM-processed Al–Zn–Mg–Cu alloy reveals the exposed surface of columnar grains, with microcracks clearly visible around the eutectics (Figure 7a). This indicates that the crack propagates along the columnar grain boundary under tensile loading, showing intergranular fracture. However, the fracture surface of LAHAM specimen becomes rough accompanied by cleavages which concludes that the failure mechanism is brittle fracture (Figure 7b). Following heat treatment, the fracture surface of LAHAM samples shows tear edges and Al_2CuMg particles (Figure 7c,d). When the specimen is under tensile stress, the Al_2CuMg phase with limited plasticity in the aluminum matrix becomes a favored site for microcrack initiation. As a result, the fracture mechanism shifts from brittle to ductile.

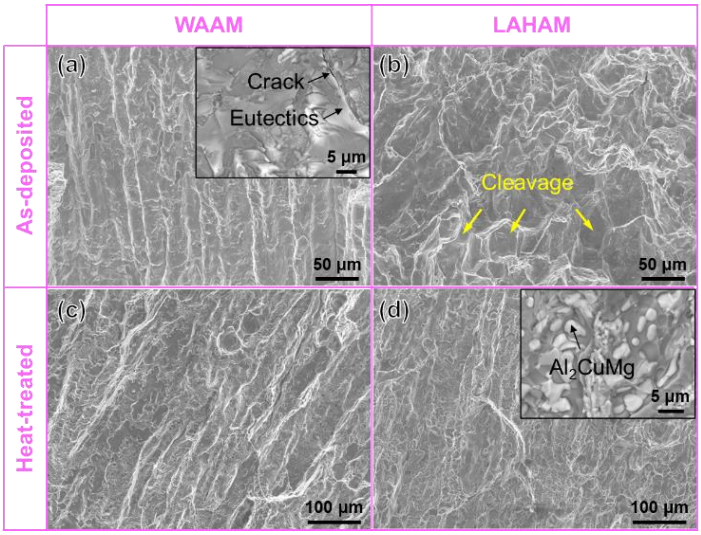

Figure 7. Fracture surfaces of WAAM specimen: **(a)** and LAHAM specimen **(b)** under deposited condition, fracture morphologies of WAAM specimen **(c)** and LAHAM specimen **(d)** under heat-treated condition.

The size and distribution of secondary phases, especially those with hard-brittle precipitates in the ductile Al matrix, are widely acknowledged to have a major impact on the mechanical properties of Al–Zn–Mg–Cu alloys [26]. The as-deposited specimen in this study demonstrates eutectic accumulation at grain boundaries, enabling cracks to spread without obstruction along these eutectic phases. By contrast, heat-treated specimen displays uniformly dispersed η' precipitates within the Al matrix. Dislocation motion is impeded by the semi-coherent interface between the η' precipitate and the α-Al phase. The strength increment induced by the Orowan mechanism from η' precipitates are as follows [27]:

$$\Delta\sigma_{or} = M\frac{0.4}{\pi}\frac{G}{\sqrt{1-\nu}}\frac{b\ln(\frac{2\sqrt{2/3}R}{b})}{[(\frac{3\pi}{4\phi})^{1/2}-1.64]R} \quad (1)$$

where M and ν are the Taylor factor and Poisson coefficient for Al, G and b represent the shear modulus and Burgers vector, respectively. R and ϕ are the average radius and volume fraction of η' precipitates. This equation means that as the small size η' precipitate increases, the stress required for dislocation slip grows, which is reflected in enhanced mechanical properties.

4. Conclusions

The Al-7.75Zn-1.46Mg-2.34Cu alloy was deposited by laser-arc hybrid process, accompanied by the investigation of microstructure evolution and mechanical properties. The main conclusions are outlined below:

(1) The microstructure in the deposited specimen features coarse columnar grains with an average size of 70.4 μm. Conversely, the LAHAM-processed Al–Zn–Mg–Cu alloy displayed a grain structure with alternating columnar grains in the AZ and equiaxed grains in the LZ. The continuously secondary phase was distributed at the boundary of columnar grain. The high-densities η' precipitates with the length of 10–30 nm appeared in the heat-treated specimen processed by LAHAM.

(2) The LAHAM-processed Al–Zn–Mg–Cu alloy had favorable UTS of 315 ± 11 MPa, which was 13% higher than that of WAAM specimen. Moreover, the UTS and elongation after heat treatment were increased of 87% and 169%, achieving values of 590 ± 9 MPa and 8.6% ± 0.2%, respectively.

Acknowledgements

The authors are grateful for the financial support from the Natural Science Foundation of Hebei Province (No. E2024203071), Science and Technology Research and Development Plan of Hebei Province (No. 23311810D).

Authors' contribution

Writing—original draft, Dehua Liu; writing—review and editing, Jiang Bi, Zhuoyun Yang and Guojiang Dong; conceptualization, Dehua Liu and Jiang Bi; software, Dehua Liu and Zhuoyun Yang; investigation, Dehua Liu and Guojiang Dong. All authors have read and agreed to the published version of the manuscript.

Conflicts of interests

The authors declare no conflict of interest.

References

[1] Mehrpouya M, Dehghanghadikolaei A, Fotovvati B, Vosooghnia A, Emamian SS, *et al.* The potential of additive manufacturing in the smart factory industrial 4.0: a review. *Appl. Sci.* 2019, 9(18):3865.

[2] Sokoluk M, Cao C, Pan S, Li X. Nanoparticle-enabled phase control for arc welding of unweldable aluminum alloy 7075. *Nat. Commun.* 2019, 10(1):98.

[3] DebRoy T, Wei HL, Zuback JS, T Mukherjee, Elmer JW, *et al.* Additive manufacturing of metallic components–process, structure and properties. *Prog. Mater. Sci*. 2018, 92:112–224.

[4] Martin JH, Yahata BD, Hundley JM, Mayer JA, Schaedler TA, *et al.* 3D printing of high-strength aluminium alloys. *Nature* 2017, 549(7672):365–369.

[5] Qi T, Zhu H, Zhang H, Yin J, Ke L, *et al.* Selective laser melting of Al7050 powder: melting mode transition and comparison of the characteristics between the keyhole and conduction mode. *Mater. Des*. 2017, 135:257–266.

[6] Fang X, Chen G, Yang J, Xie Y, Huang K, *et al.* Wire and arc additive manufacturing of high-strength Al–Zn–Mg aluminum alloy. *Front. Mater.* 2021, 8:656429.

[7] Dong B, Cai X, Lin S, Li X, Fan C, *et al.* Wire arc additive manufacturing of Al–Zn–Mg–Cu alloy: microstructures and mechanical properties. *Addit. Manuf.* 2020, 36:101447.

[8] Tan C, Li R, Su J, Du Y, Attard B, *et al.* Review on field assisted metal additive manufacturing. *Int. J. Mach. Tools Manuf*. 2023, 189:104032.

[9] Wu D, Liu D, Niu F, Miao Q, Zhao K, *et al.* Al–Cu alloy fabricated by novel laser-tungsten inert gas hybrid additive manufacturing. *Addit. Manuf.* 2020, 32:100954.

[10] Liu D, Wu D, Ge C, Lu H, Chen Z, *et al.* Superior strength of laser-arc hybrid additive manufactured Al–Zn–Mg–Cu alloy enabled by a tunable microstructure. *Addit. Manuf*. 2023, 68:103526.

[11] Gong M, Zhang S, Lu Y, Wang D, Gao M. Effects of laser power on texture evolution and mechanical properties of laser-arc hybrid additive manufacturing. *Addit. Manuf*. 2021, 46:102201.

[12] Tani G, Campana G, Fortunato A, Ascari A. The influence of shielding gas in hybrid LASER–MIG welding. *Appl. Surf. Sci.* 2007, 253(19):8050–8053.

[13] Gao M, Zeng X, Yan J, Q Hu. Microstructure characteristics of laser-MIG hybrid welded mild steel. *Appl. Surf. Sci.* 2008, 254(18):5715–5721.

[14] Sigworth GK. Fundamentals of solidification in aluminum castings. *Int. J. Metalcast.* 2014, 8(1):7–20.

[15] Read WT, Shockley W. Dislocation models of crystal grain boundaries. *Phys. Rev.* 1950, 78(3):275.

[16] Mo Y, Wang C, Zhang S, Liu X, Zha M, *et al.* Achieving high strength-ductility synergy through high-density coherent precipitation in twin-roll cast Al–Zn–Mg–Cu strips. *Mater. Sci. Eng. A* 2022, 850:143592.

[17] Chung TF, Yang Y, Huang B, Shi Z, Lin J, *et al.* Transmission electron microscopy investigation of separated nucleation and *in-situ* nucleation in AA7050 aluminium alloy. *Acta Mater.* 2018, 149:377–387.

[18] Rokhlin LL, Dobatkina TV, Bochvar NR, Lysova EV. Investigation of phase equilibria in alloys of the Al–Zn–Mg–Cu–Zr–Sc system. *J. Alloys Compd.* 2004, 367(1–2):10–16.

[19] Xiao F, Wang S, Wang Y, Shu D, Zhu G, *et al.* Niobium nanoparticle-enabled grain refinement of a crack-free high strength Al–Zn–Mg–Cu alloy manufactured by selective laser melting. *J. Alloys Compd.* 2022, 900:163427.

[20] Li L, Li R, Yuan T, Chen C, Zhang Z, *et al.* Microstructures and tensile properties of a selective laser melted Al–Zn–Mg–Cu (Al7075) alloy by Si and Zr microalloying. *Mater. Sci. Eng. A* 2020, 787:139492.

[21] Li D, Zhang Z, Li S, Yang J, Zhang S, *et al.* Microstructure, mechanical properties and fatigue crack growth behavior of an Al–Zn–Mg–Cu–Si–Zr–Er alloy fabricated by laser powder bed fusion. *Int. J. Fatigue* 2023, 172:107636.

[22] Klein T, Reiter L, Schnall M. Wire-arc additive manufacturing of Al–Zn5.5–Mg–Cu (ML7075): shifting paradigms of additive manufacture-ability. *Mater. Lett.* 2022, 313:131841.

[23] Guo Y, Han Q, Lu W, An F, Hu J, *et al.* Microstructure tuning enables synergistic improvements in strength and ductility of wire-arc additive manufactured commercial Al–Zn–Mg–Cu alloys. *Virtual Phys. Prototyping* 2022, 17(3):649–661.

[24] Dong B, Xia Y, Cai X, Lin S, Fan C. Addition of Sc in wire-based directed energy deposition of Al–Mg–Zn–Cu alloy: microalloying to refine grains and improve mechanical properties. *Addit. Manuf.* 2023, 67:103494.

[25] Ren X, Jiang X, Yuan T, Zhao X, Chen S. Microstructure and properties research of Al–Zn–Mg–Cu alloy with high strength and high elongation fabricated by wire arc additive manufacturing. *J. Mater. Process. Technol.* 2022, 307:117665.

[26] Guo W, Guo J, Wang J, Yang M, Li H, *et al.* Evolution of precipitate microstructure during stress aging of an Al–Zn–Mg–Cu alloy. *Mater. Sci. Eng. A* 2015, 634:167–175.

[27] Vo NQ, Dunand DC, Seidman DN. Improving aging and creep resistance in a dilute Al–Sc alloy by microalloying with Si, Zr and Er. *Acta Mater.* 2014, 63:73–85.